PHYSICAL REVIEW A VOLUME 17, NUMBER 3 MARCH 1978

# Photoelectron angular distributions

H. K. Tseng
*Department of Physics, National Central University, Chung-li, Taiwan, Republic of China*

R. H. Pratt and Simon Yu*
*Department of Physics and Astronomy, University of Pittsburgh, Pittsburgh, Pennsylvania 15260*

Akiva Ron
*Racah Institute of Physics, Hebrew University of Jerusalem, Jerusalem, Israel*
(Received 25 October 1977)

Relativistic, multipole, and screening effects on photoelectron angular distributions are examined using the numerical partial-wave single-electron-transition code previously applied to total cross sections. We present data on the development of relativistic and higher-multipole corrections to the nonrelativistic dipole approximation, showing that these effects are not well described by such simple factors as $1+4\beta\cos\theta$ and in fact persist to threshold in high-$Z$ elements. We trace the disappearance of screening effects on the distribution with increasing energy as screening becomes simply a multiplicative normalization effect on the total cross section, and so discuss ways to parametrize angular-distribution data. Finally, we compare theory with existing experiments, including a comprehensive comparison with all experiments at 100-eV energies and above.

## I. INTRODUCTION

We wish to give a preliminary discussion of relativistic, multipole, and screening effects on photoelectron angular distributions. We use our previous code, which has been mainly utilized for total cross sections, and with which we verified the prediction that at high energies screening is a normalization effect and angular-distribution shapes agree with point Coulomb predictions.[1] Here we will examine the energy range in which screening effects on the distribution shapes appear. At these energies and above, we believe one-electron calculations should include all effects which contribute significantly to the basic atomic cross section and should therefore agree with experiment to the extent that experiment is able to measure the basic cross section.

More recently, considerable attention has been devoted to low-energy photoelectron distributions,[2] utilizing nonrelativistic (NR) dipole approximation, in which the angular distribution may be characterized by one energy-dependent asymmetry parameter $\beta_{nL}$. The first retardation corrections to such a description have sometimes been taken as $1+4\beta\cos\theta$ for $s$ electrons. Here we will examine in some detail the relativistic and higher multipole corrections to NR dipole approximation, to assess the validity of characterizing the data by the one parameter $\beta_{nL}$. Of course, as the energies decrease and the ejected electron velocity $\beta \equiv v/c$ becomes very small, one-electron calculations cease to be quantitative and give only a qualitative guide to features.

Our work is preliminary in the sense that it is exploratory, raising more questions than it answers, and makes no attempt at a comprehensive discussion of the charge $Z$, photon energy $k$, and subshell dependenence of the distributions: any comprehensive discussion seems premature. However we believe that we have found a number of novel features and obtained a variety of insights. We have studied in detail the $K$- and $L$-shell distributions for $Z=6$, 50, and 92, as well as presenting more fragmentary data for intermediate $Z$ and for outer shells. The disappearance of screening effects with increasing energy is rather as expected, though greater effects persist for high-$Z$ elements at low energies. However, the deviations from NR dipole approximation appear much larger than anticipated in high-$Z$ elements, where large only weakly energy-dependent $\cos\theta$ corrections persist close to threshold, and there are additional energy-dependent reversals in angular-distribution shapes analogous to those associated with Cooper minima. In light-$Z$ elements the effects do vanish, not as $4\beta\cos\theta$, but as $\gamma\beta\cos\theta$, where $\gamma$ is weakly energy dependent and typically changes sign at least once in the low-$\beta$ region. The situation is quite different from the case of total cross sections, where all $\cos\theta$ terms integrate out and there is major cancellation in next order [i.e., $O(\beta^2)$] between relativistic and multipole effects.

We begin in Sec. II by summarizing the relatively well understood low-energy (nonrelativistic dipole) and high-energy (normalization screening theory) predictions for the distributions. In Sec. III we

 

examine the relativistic and multipole corrections to low-energy distributions, and in Sec. IV we examine the disappearance of screening with increasing energy. After presenting so much data on distributions, and with the expectation of more extensive and systematic tabulations of distributions in the future, it is natural that we discuss, in Sec. V, how best to represent or characterize angular-distribution data. Finally, we present in Sec. VI comparisons with the existing available experimental data.

## II. LOW-ENERGY AND HIGH-ENERGY PREDICTIONS FOR ANGULAR DISTRIBUTIONS

Following the formalism of our previous work,[1] we write the differential cross section for the atomic photoeffect as

$$d\sigma/d\Omega = (2\pi)^{-2} pE\,|M_{fi}|^2 \tag{2.1}$$

subject to energy conservation. Here $\vec{p}$ (magnitude $p$) and $E$ are the momentum and energy of the ejected photoelectron. The photoeffect matrix element is

$$M_{fi} = \left(\frac{2\pi\alpha}{k}\right)^{1/2} \int \psi_f^\dagger \vec{\alpha}\cdot\vec{\epsilon}\, e^{i\vec{k}\cdot\vec{r}} \psi_i\, d^3r, \tag{2.2}$$

where $\vec{k}$ (magnitude $k$) and $\vec{\epsilon}$ are the momentum and polarization of the incident photon, $\psi_i$ the initial bound, and $\psi_f$ the final continuum electron wave functions. This reduces in nonrelativistic dipole approximation to the simple form

$$M_{fi} = \left(\frac{2\pi\alpha}{k}\right)^{1/2} \int \psi_f^* \vec{p}\cdot\vec{\epsilon}\,\psi_i\, d^3r\,. \tag{2.3}$$

It is easy to understand the most general possible form for the angular distribution in NR dipole approximation. $|M_{fi}|^2$ must be quadratic in $\vec{\epsilon}$. If one sums over magnetic substates of the subshell from which the electron is ejected, the only other vector in $\sum|M_{fi}|^2$ is $\vec{p}$, since Eq. (2.3) unlike Eq. (2.2) does not contain $\vec{k}$ and the wave function does not depend on electron-spin direction. Remembering that $|\vec{\epsilon}|^2 = 1$, the only dependence of the scalar quantity $\sum|M_{fi}|^2$ on the direction $\vec{p}$ is of the form $A + B|\vec{p}\cdot\vec{\epsilon}|^2$, where $A$ and $B$ depend on energy and shell but not direction. This shows that the shape of the angular distribution, even for polarized photons, only depends on one parameter. Averaging over photon polarization

$$|\hat{p}\cdot\hat{\epsilon}|^2 = \tfrac{1}{2}(\hat{k}\times\hat{p})^2\,, \tag{2.4}$$

so that the unpolarized cross section is

$$\frac{d\sigma}{d\Omega} = \frac{1}{4\pi}\,\sigma_{nL}[1 - \tfrac{1}{2}\beta_{nL}P_2(\cos\theta)] \tag{2.5}$$

with the asymmetry parameter $\beta_{nL} = 2B/(3A+B)$ and $\theta$ the angle between $\hat{k}$ and $\hat{p}$. (In this paper one must be careful to distinguish the asymmetry parameter $\beta_{nL}$ from the photoelectron velocity $\beta \equiv v/c$.) We can further understand that in the special case of an $s$-wave bound state the distribution is simply proportional to $\sin^2\theta \equiv \frac{2}{3}[1 - P_2(\cos\theta)]$, or $\beta_{n0} \equiv 2$, for $M_{fi}$ must be linear in $\vec{\epsilon}$ and now the only other vector in $M_{fi}$ itself is $\vec{p}$ (for a nonrelativistic $s$ wave there is no vector associated with the magnetic substate), so $M_{fi}$ itself is of the form $C\vec{p}\cdot\vec{\epsilon}$ and $|M_{fi}|^2$ of the form $|C|^2 |\vec{p}\cdot\vec{\epsilon}|^2$, giving $\sin^2\theta$ upon averaging over photon polarization. Although we have given these arguments within the independent electron model, describing photoeffect as a single-electron transition in a screened central potential, it is evident that the conclusions are more general.

To obtain an explicit expression for $\beta_{nL}$ one may make the familiar transition from velocity to coordinate form by taking the matrix element of the operater identity

$$[\vec{r}, H] = [\vec{r}, p^2/2m] = i\vec{p}$$

obtaining

$$\int \psi_f^* \vec{p}\cdot\vec{\epsilon}\,\psi_i\, d^3r = -i\int \psi_f^* \{\vec{r}H - H\vec{r}\}\cdot\vec{\epsilon}\,\psi_i\, d^3r$$
$$= ik\int \psi_f^* \vec{r}\cdot\vec{\epsilon}\,\psi_i\, d^3r\,. \tag{2.6}$$

If for $\vec{r}$ we use a spherical polar coordinate system $(r, \theta', \phi')$ with the direction $\vec{p}$ as polar axis and describe $\vec{\epsilon}$ in such coordinates by $(|\vec{\epsilon}| \equiv 1, \theta'', \phi'' \equiv 0)$, where $\theta''$ is the angle between $\vec{p}$ and $\vec{\epsilon}$, then

$$\vec{r}\cdot\vec{\epsilon} = r(\cos\theta''\cos\theta' + \sin\theta''\sin\theta'\cos\phi')\,.$$

In partial waves, bound and continuum wave functions are written as

$$\psi_i(\vec{r}) = R_{nL}(r)Y_{LM}(\hat{r})\,, \tag{2.7}$$

$$\psi_f(\vec{r}) = \sum_{l=0}^{\infty} (2l+1) i^l e^{-i\delta_l} R_{pl}(r) P_l(\hat{p}\cdot\hat{r}), \tag{2.8}$$

where the $R$'s satisfy radial Schrödinger equations and the $\delta_l$ are scattering phase shifts. Substituting Eqs. (2.6)–(2.8) into Eq. (2.3) and Eq. (2.1) and using the recurrence relations and the orthogonality properties for spherical harmonics, one obtains[3] the cross section $d\sigma/d\Omega$ by averaging over initial state and summing over final-state polarizations:

$$\left\langle \frac{d\sigma}{d\Omega} \right\rangle = \frac{\alpha p}{2\pi k}\left\langle \left| \int \psi_f^* \vec{p}\cdot\vec{\epsilon}\,\psi_i\, d^3r \right|^2 \right\rangle = \frac{\sigma_{nL}}{4\pi}[1 - \tfrac{1}{2}\beta_{nL}P_2(\cos\theta)]\,. \tag{2.9}$$

Here the total subshell photoeffect cross section

$$\sigma_{nL} = \frac{4\pi\alpha kp}{3(2L+1)}[LR_{L-1}^2 + (L+1)R_{L+1}^2] \tag{2.10}$$

and the photoelectron asymmetry parameter

$$\beta_{nL}=\frac{L(L-1)R^2_{L-1}+(L+1)(L+2)R^2_{L+1}-6L(L+1)R_{L-1}R_{L+1}\cos(\delta_{L+1}-\delta_{L-1})}{(2L+1)[LR^2_{L-1}+(L+1)R^2_{L+1}]}, \tag{2.11}$$

where the radial matrix elements

$$R_l(p)\equiv\int_0^\infty R_{pl}(r)r^3R_{nL}(r)\,dr \tag{2.12}$$

(the notation suppresses the dependence on subshell $nL$).

For the point-Coulomb $2p$ case the exact nonrelativistic dipole result of Schur[4] is

$$\left\langle\frac{d\sigma}{d\Omega}\right\rangle\propto 1+\frac{4\epsilon_L}{k}\sin^2\theta$$

or

$$\beta_{21}=\frac{16\epsilon_L}{3k+8\epsilon_L}. \tag{2.13}$$

Note that this varies from $\beta_{21}=\frac{16}{11}$ at threshold to 0 (isotropic distribution) at high energies. The latter is in accord with the result of Bethe and Salpeter[5] that for $p$ waves in the Born approximation (i.e., high NR energy) $\beta_{nL}=0$, for any potential.

There has been considerable work[6] on the energy dependence of $\beta_{nL}$ within the independent-particle model. Except for the $\beta_{n0}\equiv 2$ it is found that the $\beta_{nL}$ vary rapidly near threshold. The energy dependence of $\beta_{nL}$, and hence of the angular distribution, for a given subshell is greatly affected by the presence (or absence) of a Cooper minimum in the corresponding cross section. These minima occur only in $l=L+1$ channels for outer and near outer shells. Recent work has indicated that near threshold the independent-particle model is adequate for closed-shell atoms except in the vicinity of a Cooper minimum but not generally for open-shell atoms. At higher energies, as we shall be demonstrating in this paper, the deviations from nonrelativistic dipole approximation must be considered.

When we turn to the higher-energy relativistic region, beyond specific numerical or approximate analytical calculations, the only insight which has been achieved is associated with the normalization screening theory.[7] What has been realized is that in this situation the minimum momentum transfer to the atom $q_{\min}\sim\lambda\!\!\!^{-}_e{}^{-1}$, providing an effective cutoff for the matrix-element integrand at electron Compton wavelength distances $r\sim\lambda\!\!\!^{-}_e$. At such small distances all wave-function shapes are point Coulombic and screening enters only through wave-function normalizations. Cross sections differ from point-Coulomb cross sections only due to differences in the squares of normalization constants: the shapes of angular distributions (as well as polarization correlations) are the same as for the point-Coulomb case. These predictions have been verified in numerical calculations.[1]

In the relativistic region similar arguments relate distributions from states of same $K[K=\mp(J+\frac{1}{2})$ and $J=L\pm\frac{1}{2}]$, different $n$, as for example $1s$ and $2s$. This follows because at such small distances the shape of a wave function is independent of $n$, and the value of $n$ enters the matrix element only through the wave-function normalization. Once again, the ratio of cross sections measures the square of the ratios of normalizations; angular-distribution shapes (and polarization correlations) do not depend on $n$ for a given $K$. These predictions have also been verified in numerical calculations and in experiments.[1]

A relativistic Born approximation prediction ($Z\alpha\ll\beta$) is available for the point-Coulomb $K$-shell angular distribution—the Sauter formula[8]

$$\left(\frac{d\sigma}{d\Omega}\right)_{\text{Sauter}}=\lambda(1-\beta\cos\theta)^{-4}\sin^2\theta\times[1+\tfrac{1}{2}k(k^2-1)(1-\beta\cos\theta)], \tag{2.14}$$

where

$$\lambda=a^5\alpha 4\beta(k+2)/k^4(k+1)^3.$$

(From the previous discussion it is evident that this shape is also obtained for the $L_I$ distribution.) In the nonrelativistic limit, keeping $Z\alpha\ll\beta$, $k\to\frac{1}{2}\beta^2$, and the Sauter formula reduces to $\lambda\sin^2\theta$, in agreement with the nonrelativistic dipole-approximation result (not restricted to Born approximation). Note that the first corrections to this limit are $O(\beta)$, due to the $(1-\beta\cos\theta)^{-4}$, and of the form $(1+4\beta\cos\theta)$. For high energies $(1-\beta\cos\theta)^{-3}$ dominates in the Sauter formula and, following Bethe and Salpeter, the distribution, strongly peaked forward, behaves for small angles as

$$16a^5\alpha\gamma^3\theta^2(1+\gamma^2\theta^2)^{-3},$$

with

$$\gamma=1/(1-\beta^2)^{1/2}.$$

The Sauter formula vanishes in the forward (and backward) directions. However, both analytic and numerical calculations show both in point-Coulomb and screened cases the presence of nonvanishing terms of relative order $(Z\alpha)^2$ in the forward direction. For high $Z$'s and high energies the minimum in the forward direction is completely filled in.[9]

## III. RELATIVISTIC AND MULTIPOLE CORRECTIONS TO LOW-ENERGY ANGULAR DISTRIBUTIONS

The photoelectron angular distribution may be characterized by the coefficients $B_n$ in a Legendre expansion

$$\frac{d\sigma}{d\Omega}=\frac{\sigma}{4\pi}\sum_{n=0}^{\infty}B_nP_n(\cos\theta),$$

where $\sigma$ is the total cross sections and $B_0\equiv 1$. In Figs. 1 and 2 we give our numerical results for the energy dependence of the $B_n$ in a variety of cases; the series converge within a few terms at low and intermediate energies. These results, which we examine further below, may be contrasted with the nonrelativistic dipole prediction that *only* $B_0$ and $B_2$ are nonzero, and that for ejection from an $s$ state $B_2\equiv -1$.[3] (Deviations from these predictions when one goes beyond central-field approximation have recently been discussed by Starace, Rast, and Manson.[10])

Corrections to nonrelativistic dipole approximation result both from relativistic effects and from higher multipoles. There are relativistic corrections to wave functions in $Z\alpha$ as well as in $\beta$, so that in addition to modifications at relativistic energies there can be modifications in heavy elements persisting to threshold. However in relativistic dipole approximation, summing and averaging electron spins, it is clear that the previous argument for the general form of the angular distribution still applies, so that only $B_0$ and $B_2$ are nonzero. Due to the spin variables one can no longer argue that $B_{n0}=2$, and this consequence of relativistic dipole approximation has been discussed by Walker and Waber.[11] But nonzero values for the other $B_n$'s, as in Figs. 1 and 2, result from higher-order terms in the multipole expansion.

The multipole expansion is an expansion in $\vec{k}\cdot\vec{r}$. Retracing the previous argument with these additional vectors, it is clear that the cross term from the $l$th multipole will contain additional angular dependence through $\cos^l\theta$ leading to nonvanishing $B$'s through $B_{2+l}$. In particular, the first multipole correction will give corrections to the cross section proportional to $\hat{k}\cdot\hat{p}\equiv\cos\theta\equiv P_1(\cos\theta)$, or a differential cross section

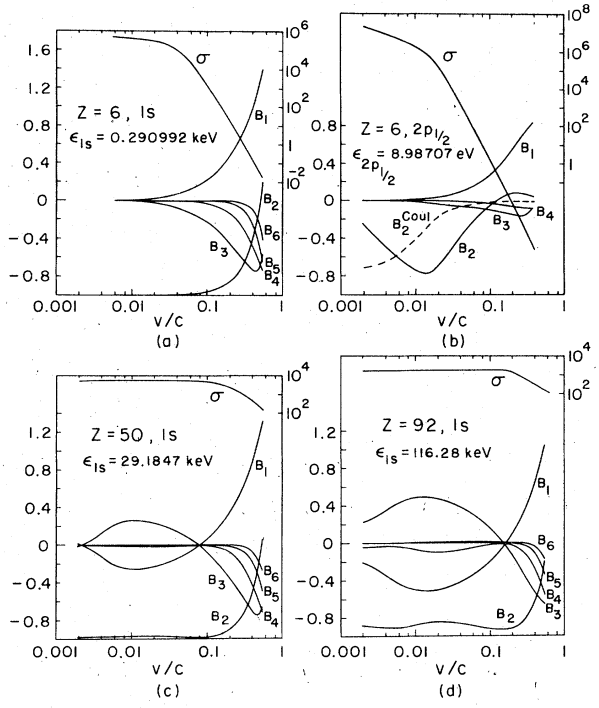


FIG. 1. Coefficient $B_n$ as a function of $v/c$ for photoeffect from (a) $Z=6$, $1s$; (b) $Z=6$, $2p_{1/2}$; (c) $Z=50$, $1s$; and (d) $Z=92$, $1s$. In each case the total cross section $\sigma$ is also shown. In (b) we have also shown the nonrelativistic Coulomb dipole prediction for $B_2$ (dashed curve). Note that in each case the right-hand scale is for $\sigma$ (in barns/atom), while the left-hand side is for $B_n$'s.

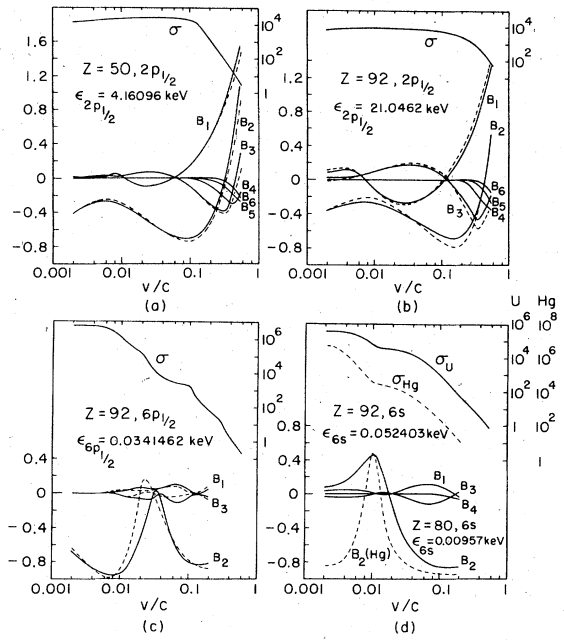


FIG. 2. Coefficient $B_n$ as a function of $v/c$ for photoeffect from (a) $Z=50$, $2p_{1/2}$; (b) $Z=92$, $2p_{1/2}$; (c) $Z=92$, $6p_{1/2}$; and (d) $Z=92$, $6s$. In each case the total cross section $\sigma$ is also shown. In (a), (b), and (c) we have also shown the corresponding $2p_{3/2}$ predictions (dashed curves). In (d) we have also shown $\sigma$ and $B_2$ for $Z=80, 6s$ (dashed curves). Note that in each case the right-hand scale is for $\sigma$ (in barns/atom), while the left-hand scale is for $B_n$'s.

$$\frac{d\sigma}{d\Omega}=\frac{\sigma}{4\pi}[1+B_2P_2(\cos\theta)+\cos\theta(C+D\sin^2\theta)]$$

$$\equiv\frac{\sigma}{4\pi}\sum_{i=0}^{3}B_iP_i(\cos\theta)\,.$$

Again, in the nonrelativistic (but not the relativistic) bound $s$-state case, since there are no other vectors, the NR dipole matrix element is proportional to $\vec{\epsilon}\cdot\vec{p}$ and the first multipole correction to $\vec{\epsilon}\cdot\vec{p}\,\hat{k}\cdot\hat{p}$, giving a cross section $\sin^2\theta(1+\gamma\cos\theta)$, or $B_2=-1$ and $B_1=-B_3$. Deviations of relativistic origin from both predictions are to be expected in high-$Z$ elements even near threshold.

There are a few analytic results in the Coulomb potential which go beyond nonrelativistic dipole approximation and offer some insight into the nature of these corrections. Best known is the multiplicative factor $(1+4\beta\cos\theta)$ derived for the $K$ shell, this form in accord with our general arguments with $\gamma\equiv4\beta$. For future reference we note that it corresponds to $B_0=-B_2=1$, $B_1=-B_3=-\frac{12}{5}\beta$, $B_n=0$ for $n\geq4$. The simplest way to derive this result is in nonrelativistic Born approximation,[12] letting $\psi_i=(a^3/\pi)^{1/2}e^{-ar}$ and $\psi_f=e^{i\vec{p}\cdot\vec{r}}$ in the nonrelativistic matrix element with retardation

$$M_{fi}=\left(\frac{2\pi\alpha}{k}\right)^{1/2}\int\psi_f^*e^{i\vec{k}\cdot\vec{r}}\vec{\epsilon}\cdot\vec{p}\psi_i\,d^3r\,,$$

obtaining

$$\frac{d\sigma}{d\Omega}=\frac{16\alpha a^5}{kp^5}\frac{\sin^2\theta}{(1-\beta\cos\theta)^4}\,,$$

which on expansion in $\beta$ gives the corrective factor $(1+4\beta\cos\theta)$. The same result is obtained in a small-$Z$ expansion of the relativistic Born-approximation Sauter formula[8] Eq. (2.16) [since $k=0(\beta^2)$ in Born approximation the second term can be dropped], showing that the corrective factor is indeed a higher multipole rather than a relativistic effect, as we had indicated previously. The exact NR Coulomb $K$-shell result with retardation was obtained by Fischer[13] and Sauter, using the continuum Coulomb wave function for $\psi_f$ above; the result differs from Born approximation only in replacing $(1-\beta\cos\theta)^{-4}$ by $(1+\frac{1}{2}k-\beta\cos\theta)^{-4}$. Since $2k=a^2+\beta^2$ for the $K$ shell, this will yield the Born-approximation correction for $a\ll\beta$, but no correction for $a\gg\beta$ as $\beta\to0$. It is clear that the conclusion $\gamma=4\beta$ is a low-$Z$ point-Coulomb result. As our numerical results show, screening effects will change the coefficient from 4 and for high $Z$ there are large corrections even near threshold.

Schur[4] has given nonrelativistic Coulomb results for the $L$ shell, for $2s$ the distribution

$$\sin^2\theta[1+4\beta(1-\epsilon_L/k)\cos\theta]\,,$$

and for $2p$

$$[1+2\beta\cos\theta]+\sin^2\theta\left[\frac{4\epsilon_L}{k}+2\beta\left(1+\frac{11\epsilon_L}{k}\right)\cos\theta\right],$$

or

$$\left(1+\frac{8\epsilon_L}{3k}\right)B_i=\frac{2\beta}{5}\left(7+\frac{22\epsilon_L}{k}\right),\ \frac{-8\epsilon_L}{3k},\ \frac{-4\beta}{5}\left(1+\frac{11\epsilon_L}{k}\right),$$

for $i=1,2,3$, respectively.

This $2s$ correction vanishes at threshold and coincides with the $1s$ correction at high energies, the latter feature in agreement with the prediction of the normalization screening theory. The $2p$ corrections are not isotropic at high energies.[14]

Let us now examine Figs. 1 and 2 in view of our discussion. In each case we have plotted the leading $B_n$ as a function of electron velocity $\beta$ on a logarithmic scale; we also show the total cross section at the top of each figure. The cross sections are roughly constant until the continuum electron kinetic energy becomes comparable with the binding energy of the initial electron and then begin to drop rapidly; this corresponds to the transition from a matrix-element integrand cut off by the bound state (continuum wave independent of energy in the interior) and an integrand cut off by the continuum state at increasingly short distances as the energy and frequency of oscillation increases.

Figure 1(a) shows results for the $K$ shell of carbon ($Z=6$, $1s$), a low-$Z$ case for which we would not expect important relativistic effects at threshold. When the cross section is constant $B_2=-1$ and all other $B$'s are very small, in agreement with NR dipole approximation. $B_1=B_3=\frac{12}{5}\beta$ in agreement with the Coulomb prediction of the higher-multipole correction, even for $\beta$ as large as 0.2 or 0.3. This shows that screening has little effect at any energy on such a low-$Z$ $s$-wave case, where the NR dipole limit is independent of potential and at high energies since screening is a normalization effect it again does not affect the distribution. The deviation of $B_2$ from $-1$ appears to develop as $\beta^2$, also consistent with our previous discussion, and the higher $B_n$'s indeed develop more slowly.

Next, in Fig. 1(b) we look at ($Z=6$, $2p_{1/2}$), still low $Z$ but no longer $s$ wave. The binding energy is low and we do not see the region of constant cross section, but all except $B_2$ are indeed vanishing. Now screening effects are important at low energy (unlike the $s$-wave case) and $B_2$ does not agree with Schur's point-Coulomb value (as shown). The minimum value of $B_2$ is close to Schur's $-\frac{8}{11}$ threshold prediction (a feature we will also see in the higher $Z$ cases) and for $\beta\sim0.1$,

where screening effects may be unimportant and NR dipole still qualitatively correct. $B_2$ is small in agreement with Schur. $B_1 \neq -B_3$ and for $\beta \sim 0.1$ are also consistent with Schur's point-Coulomb prediction.

In Figs. 1(c) and 1(d) we study $Z$ dependence, contrasting the low-$Z$ $K$-shell data of Fig. 1(a) with higher-$Z$ $K$-shell data for $(Z=50, 1s)$ and $(Z=92, 1s)$. It is evident that for high $Z$ $O(a^2)$ deviations from NR dipole approximation persist to threshold. $B_2$ is not $-1$ and $B_1$ and $B_3$ do not vanish. $B_4$ also remains finite, perhaps $O(a^3)$. We still fairly well observe $B_1 = -B_3$, presumably because the deviation from $B_2 = -1$ is not large and the main correction term is still of the type $\sin^2\theta\cos\theta$. In the low-energy regime $B_1$ is pulled negative, which has the interesting consequence that the angular distribution will peak *backward* from 90°, as in Figs. 1(c) and 1(d). Thus for a high-$Z$ $K$ shell, as we decrease the incident photon energy, the photoelectron angular distribution, first strongly peaked forward (at high energies) will shift towards 90° and, by 10 keV above threshold, begin to peak backward. In this single-electron calculation the shift would be most pronounced about 3 keV above threshold. It is interesting to note that this occurs at energies for which the cross section is constant.

In a similar way, Figs. 2(a) and 2(b) permit us to study the $Z$ dependence of $p$ states, contrasting the low $Z$ data of Fig. 1(b) with $(Z=50, 2p_{1/2})$ and $(Z=92, 2p_{1/2})$. Deviations from NR dipole approximation, though smaller than in the $s$-wave case, again persist to threshold. In these high-$Z$ cases $B_1$ is pulled below zero, as for $s$ waves. There seems to be a correlation between the minimum of $B_2$ and the zeroes of $B_1$ and $B_3$. And as already noted, the magnitude of the minimum of $B_2$ is similar to that predicted by Schur. Figures 2(a) and 2(b) also allow us to inspect the effects of spin-orbit coupling, as we have also plotted the corresponding $2p_{3/2}$ data. These effects, discussed for $B_2$ by Walker and Waber,[11] are not large; as expected they are most visible for $Z=92$ (for $Z=6$, $2p_{1/2}$ and $2p_{3/2}$ are most identical).

Figures 2(c) and 2(d) give some examples of outer-shell results in this single-electron model, to indicate the wealth of information available for analysis. Figure 2(c) gives $6p_{1/2}$ and $6p_{3/2}$ data for $Z=92$. The cross section appears to have considerable structure, associated with rapid variation in the $B_n$'s. Near $\beta \sim 0.03$ $B_2$ goes through a sharp maximum and the deviations between $6p_{1/2}$ and $6p_{3/2}$ are largest. Figure 2(d) shows $6s$ data for $Z=92$, again with structure in the cross sections and the $B_n$'s. Unlike the $6p$ case, deviations from NR dipole approximation persist to threshold. Most striking is the gross deviation in $B_2$ from $-1$, including a change of sign and a maximum. This could be an example of the relativistic effect for $S$ orbitals described by Walker and Waber, and requires that the transition matrix elements to continuum $p_{3/2}$ and $p_{1/2}$ states be very different near Cooper minima. Figure 2(d) also shows $6s$ data for Hg, relevant to the experiment of Niehaus and Ruf.[15] There is a similar structure in $B_2$ but at lower energies it returns to dipole form. The other $B_n$'s remain small.

## IV. SCREENING CORRECTIONS AT INTERMEDIATE ENERGIES

We have already described the argument that at high energies screening enters only as a normalization factor and so does not affect angular-distribution shapes, and we have noted the numerical calculations which support this assertion. We do not yet have a quantitative analytic theory to characterize the development of deviations from this simple description at intermediate energies. The elements of such a theory are being developed: in the nonrelativistic case we have an analytic-perturbation theory for screened wave functions of definite angular momentum.[16] This has been used to calculate the development of screening effects in the NR dipole matrix element.[17] A similar treatment of relativistic partial waves is being completed,[18] and work on a nonrelativistic wave function of definite asymptotic linear momentum is in progress.[19] However what will really be needed is an analytic relativistic screened wave function of definite asymptotic linear momentum.

Meantime, we can discuss the implications of the normalization screening theory, and deviations from it at intermediate energies, for the calculation of the photoeffect matrix element in partial waves. At both high and intermediate energies, the matrix element for inner shells is determined at rather small distances, where bound and continuum shapes are point Coulomb. Screening of the bound state enters only through its normalization; this effect is a constant, independent of energy, larger for low $Z$ and outer shells; it has no effect on angular-distribution shapes, only on the total cross section. Screening effects from the continuum states enter the total cross section only through the normalization $N_\kappa$; they enter the angular distribution also through the phase shifts $\delta_\kappa$. Screening effects also enter the matrix element through the external factor $(pE)^{1/2}$ of Eq. (2.1), for, since screening shifts the bound-state energy, it also shifts the continuum $p$ resulting from a photon of given $k$. We see from the examples of Tables I and II that the $\tilde{N}_\kappa \equiv (pE)^{1/2} N_\kappa$ are quite inde-

TABLE I. $\kappa, k$ dependence of relative normalizations and phases for photoeffect from $Z=6$, $1s$; $\epsilon_c = 0.490\,04$ keV, $\epsilon_{HFS} = 0.290\,99$ keV.

| $k$ | 0.6 keV | | 1.0 keV | | 5.0 keV | | 5.0 keV | |
|---|---|---|---|---|---|---|---|---|
| $\kappa$ | $\tilde{N}_s/\tilde{N}_c$ | $\delta_s-\delta_c$ | $\tilde{N}_s/\tilde{N}_c$ | $\delta_s-\delta_c$ | $\tilde{N}_s/\tilde{N}_c$ | $\delta_s-\delta_c$ | $\tilde{N}_s/\tilde{N}_c$ | $\delta_s-\delta_c$ |
| −5 | 1.651 | 0.780 | 1.101 | 2.121 | 0.994 | 0.979 | 0.999 | 0.436 |
| −4 | 1.236 | 0.482 | 1.030 | 2.027 | 0.993 | 0.970 | 0.999 | 0.436 |
| −3 | 1.023 | 0.168 | 0.990 | 1.938 | 0.994 | 0.962 | 0.999 | 0.436 |
| −2 | 0.974 | 0.094 | 0.983 | 1.865 | 0.997 | 0.957 | 1.000 | 0.436 |
| −1 | 1.004 | 0.197 | 1.002 | 1.838 | 1.000 | 0.956 | 1.000 | 0.436 |
| 1 | 0.974 | 0.094 | 0.983 | 1.865 | 0.997 | 0.957 | 1.000 | 0.436 |
| 2 | 1.023 | 0.167 | 0.990 | 1.938 | 0.994 | 0.962 | 0.999 | 0.436 |
| 3 | 1.236 | 0.482 | 1.030 | 2.027 | 0.993 | 0.970 | 0.999 | 0.436 |
| 4 | 1.651 | 0.780 | 1.101 | 2.121 | 0.994 | 0.979 | 0.999 | 0.436 |
| 5 | 2.339 | 1.048 | 1.204 | 2.211 | 0.997 | 0.989 | 0.998 | 0.437 |

pendent of screening, particularly for low $\kappa$'s, and approach the Coulomb values at high energy for all $\kappa$; this was noted empirically and later explained (in the NR case) via the analytic perturbation theory.[16] Thus, in the high-energy case, when many $\kappa$'s contribute to the total cross section, screening enters only through the bound-state normalization. Deviations of $(pE)^{1/2}N_\kappa$ from point Coulomb remain small down into the NR (small $\beta$) region. There the deviations begin to grow for large $\kappa$, but the contribution of such $\kappa$'s to the cross section is becoming small. Thus screening effects (other than bound-state normalization) on the total cross sections remain small down to very low energies, as Oh *et al.*[17] have found in an NR calculation. This argument is really made for a bound $s$-wave case; when large-$\kappa$ partial waves dominate at low energy, significant screening effects will develop.

To discuss angular distributions one must also consider the phase shifts $\delta_\kappa$, also shown in Tables I and II. Because of the logarithmic phase factor of the long-range point-Coulomb case, one cannot expect screened phases to approach Coulomb phases of high energies. However the difference becomes an energy-dependent $\kappa$-independent constant, i.e., an overall phase which does not affect the differential cross section. The deviations of $\delta_\kappa$(screened) $-\delta_k$ (Coulomb) from $\kappa$ independence follow the same pattern as the screening dependence of the normalizations, and so the same statements apply to the screening dependence of the angular distribution and the total cross section. However, we should remember that, for bound $s$ waves at low energies, if $(Z\alpha)^2$ may also be neglected (NR dipole approximation), the angular distribution is the same—$\sin^2\theta$—in any potential and screening will only affect the total cross section. For the low-$Z$ case we also saw in the previous section that when $\beta$ is large enough the retardation corrections $O(\beta)$ should not be neglected but $O(\beta^2)$ still may. The $O(\beta)$ retardation term has approached its point-Coulomb value, and so the distribution retains point-Coulomb form as long as $O(\beta^2)$ and $O(Z\alpha)^2$ may be neglected.

For a qualitative understanding of the angular

TABLE II. $\kappa, k$ dependence of relative normalizations and phases for photoeffect from $Z=92$, $1s$; $\epsilon_c = 132.28$ keV, $\epsilon_{HFS} = 116.29$ keV.

| $k$ | 150.0 keV | | 200.0 keV | | 250.0 keV | | 500.0 keV | |
|---|---|---|---|---|---|---|---|---|
| $\kappa$ | $\tilde{N}_s/\tilde{N}_c$ | $\delta_s-\delta_c$ | $\tilde{N}_s/\tilde{N}_c$ | $\delta_s-\delta_c$ | $\tilde{N}_s/\tilde{N}_c$ | $\delta_s-\delta_c$ | $\tilde{N}_s/\tilde{N}_c$ | $\delta_s-\delta_c$ |
| −5 | 1.204 | 0.281 | 1.056 | 1.221 | 1.027 | 0.681 | 1.002 | 0.114 |
| −4 | 1.082 | 0.124 | 1.023 | 1.175 | 1.010 | 0.654 | 0.999 | 0.106 |
| −3 | 1.014 | −0.021 | 1.002 | 1.131 | 0.999 | 0.629 | 0.997 | 0.098 |
| −2 | 0.995 | −0.131 | 0.996 | 1.096 | 0.996 | 0.609 | 0.998 | 0.092 |
| −1 | 0.999 | −0.179 | 1.000 | 1.080 | 1.000 | 0.600 | 1.000 | 0.090 |
| 1 | 0.995 | −0.140 | 0.997 | 1.145 | 0.997 | 0.604 | 0.999 | 0.090 |
| 2 | 1.007 | −0.030 | 0.999 | 1.125 | 0.997 | 0.624 | 0.997 | 0.095 |
| 3 | 1.072 | 0.116 | 1.018 | 1.168 | 1.006 | 0.649 | 0.998 | 0.102 |
| 4 | 1.192 | 0.275 | 1.049 | 1.215 | 1.022 | 0.675 | 1.000 | 0.110 |
| 5 | 1.373 | 0.436 | 1.092 | 1.262 | 1.044 | 0.703 | 1.005 | 0.119 |

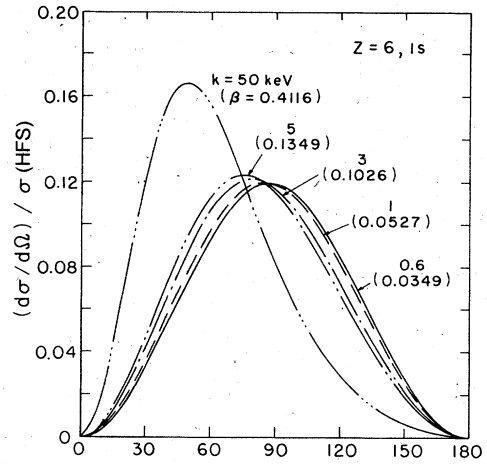


FIG. 3. Predicted normalized angular distribution of photoelectrons $(d\sigma/d\Omega)/\sigma$ (HFS) from $Z=6$, $1s$, as a function of photon energy $k$.

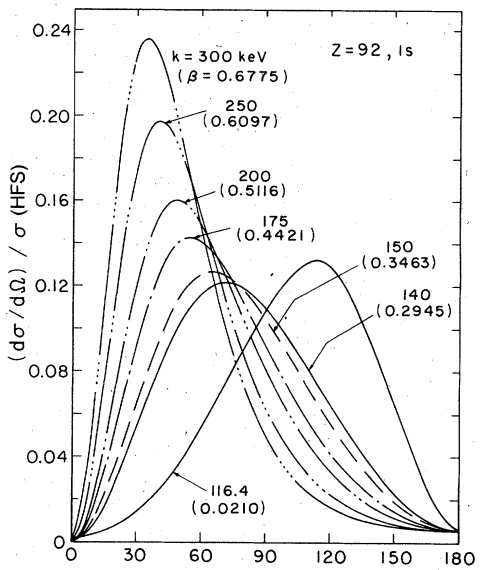


FIG. 5. Predicted normalized angular distribution of photoelectrons $(d\sigma/d\Omega)/\sigma$ (HFS) from $Z=92$, $1s$, as a function of photon energy $k$. Note the backward peaking of the distribution at very low energies.

distributions we show in Figs. 3–7 $(d\sigma/d\Omega)/\sigma$(HFS) as a function of angle, energy, $Z$, and subshell. We give in Tables III and IV the deviations from point-Coulomb shapes. Deviations in angular distributions are described by the parameter

$$NE(\theta)=\frac{\sigma_{\rm HFS}}{\sigma_{\rm C}}\frac{\sigma_{\rm C}(\theta)}{\sigma_{\rm HFS}(\theta)}-1,$$

where $\sigma(\theta)$ is the photoeffect angular cross section. The subscripts C and HFS refer to the point-Coulomb and the Hartree-Fock-Slater potentials, respectively. Deviations in the total cross sections are characterized by

$$NE=\frac{\Xi^2_{\rm HFS}}{\sigma_{\rm HFS}/\sigma_{\rm C}}-1,$$

where $\Xi^2_{\rm HFS}$ is the ratio of screened to point-Coulomb bound-state normalizations. For low $Z$ these deviations are small, always small for $s$ waves, for $2p$ growing near threshold. For high $Z$ effects are large at intermediate energies, and gradually decline with increasing energies. Note that these effects in $Z$ are large only for the angular distribution—the screening effects on total cross sections remain small, in agreement with the NR calculation of Oh *et al.*[17] Presumably this arises because the $Z$-dependent deviations of $\delta_\kappa$(sc)

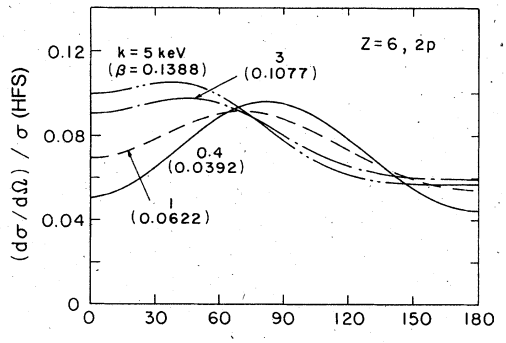


FIG. 4. Predicted normalized angular distribution of photoelectrons $(d\sigma/d\Omega)/\sigma$ (HFS) from $Z=6, 2p$, as a function of photon energy $k$.

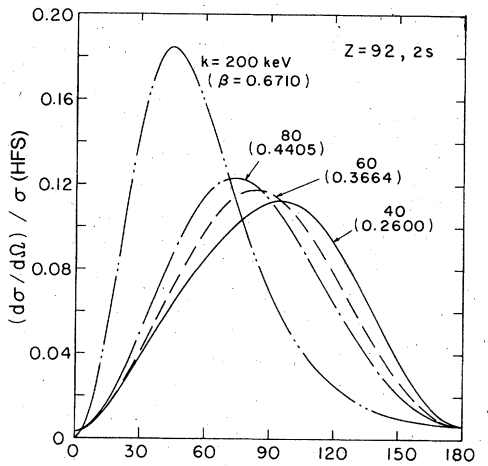


FIG. 6. Predicted normalized angular distribution of photoelectrons $(d\sigma/d\Omega)/\sigma$ (HFS) from $Z=92$, $2s$ as a function of photon energy $k$.

TABLE III. Deviations from point-Coulomb shapes $Z=6$.

| $\theta$ (deg) \ $NE(\theta)$ for | 1s $k=0.6$ keV | 1s $k=5$ keV | 1s $k=50$ keV | 2s $k=0.4$ keV | 2s $k=5$ keV | 2p $k=0.4$ keV | 2p $k=5$ keV |
|---|---|---|---|---|---|---|---|
| 0 | 0.257 | 0.049 | −0.000 | 0.263 | −0.118 | −0.079 | −0.008 |
| 10 | −0.020 | 0.005 | −0.001 | −0.000 | 0.007 | −0.072 | −0.006 |
| 20 | −0.019 | 0.005 | −0.001 | −0.000 | 0.007 | −0.054 | −0.003 |
| 40 | −0.015 | 0.004 | −0.001 | −0.000 | 0.005 | −0.014 | 0.005 |
| 60 | −0.010 | 0.002 | −0.000 | −0.000 | 0.003 | 0.012 | 0.007 |
| 90 | 0.001 | −0.001 | 0.001 | 0.000 | −0.001 | 0.019 | 0.002 |
| 120 | 0.010 | −0.003 | 0.001 | −0.000 | −0.004 | −0.001 | −0.008 |
| 150 | 0.017 | −0.004 | 0.001 | −0.000 | −0.007 | −0.044 | −0.014 |
| 180 | 0.273 | 0.032 | 0.000 | 0.246 | −0.169 | −0.076 | −0.013 |
| $\sigma_{HFS}$ (b/atom) | 167 800 | 353.8 | 0.1972 | 20 010 | 18.23 | 2408 | 0.1872 |
| $\sigma_{HFS}/\sigma_c$ | 0.8299 | 0.9136 | 0.9175 | 0.3634 | 0.3993 | 0.1497 | 0.1638 |
| $\Xi^2_{HFS}$ | 0.9130 | 0.9130 | 0.9130 | 0.3933 | 0.3933 | 0.1613 | 0.1613 |
| $NE$ | 0.100 | −0.001 | −0.005 | 0.082 | −0.015 | 0.078 | −0.015 |

$-\delta_\kappa$(Coul) are larger than those of $(pE)^{1/2}N_\kappa$, and because higher partial waves (as cross terms) contribute more to angular distributions than to total cross sections, but full elucidation of the phenomena may require completion of the analytic theory.

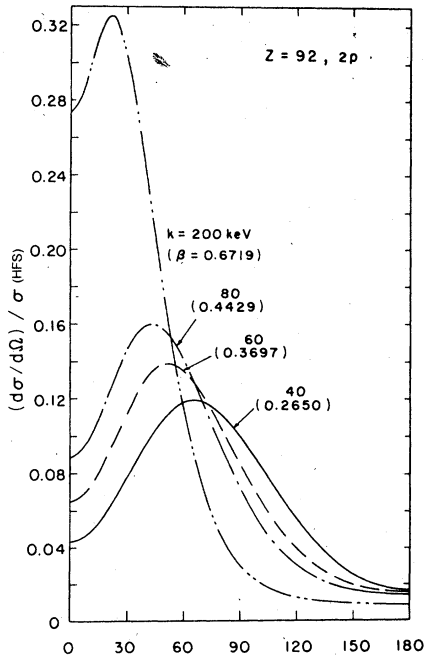


FIG. 7. Predicted normalized angular distribution of photoelectrons $(d\sigma/d\Omega)/\sigma$(HFS) from $Z=92$, $2p$, as a function of photon energy $k$.

## V. REPRESENTATION AND TABULATION OF DISTRIBUTIONS

Representations are needed for systematic tabulation of angular-distribution data. For theory as well, it is desirable to identify a small number of parameters which characterize the distributions. One can of course display angular distribution on some mesh in $\theta$, which gives immediate intuitive understanding. However effort is needed for interpolation in $\theta,k,Z$. We have seen that the coefficients of a $P_l$ expansion, the $B_l$, are useful to characterize data in the low-$\beta$ region (and intermediate). However at higher energies such series converge very slowly, owing to forward peaking, and do not really display independent parameters. The form of the Sauter formula suggest a representation such as

$$\frac{d\sigma}{d\Omega}=\frac{\sigma}{4\pi}A\frac{\sum_l B_n(l)P_l(\cos\theta)}{(1-\gamma\beta\cos\theta)^n}, \tag{5.1}$$

where $A$ is defined by

$$\sigma=\frac{d\sigma}{d\Omega}d\Omega .$$

For the Sauter formula with $\gamma=1$ and $n=4$ the representation takes the simple form

$$(1+\delta)A^{-1}=(1-\beta^2)^{-2}+\frac{3\delta}{2\beta^2(1-\beta^2)}\left(1-\frac{1-\beta^2}{2\beta}\ln\frac{1+\beta}{1-\beta}\right),$$

$$B_4(0)=-B_4(2)\equiv 1,$$

$$B_4(1)=-B_4(3)=-\tfrac{3}{5}\frac{\delta\beta}{1+\delta},\quad \delta\equiv\tfrac{1}{2}k(k^2-1),$$

$$B_4(l)=0,\quad l>3.$$

There is some ambiguity whether to take $\gamma=1$,

TABLE IV. Deviations from point-Coulomb shapes $Z=92$.

| $\theta$ (deg) \ $NE(\theta)$ for | $1s$ $k=140$ keV | $1s$ $k=200$ keV | $1s$ $k=300$ keV | $2s$ $k=40$ keV | $2s$ $k=200$ keV | $2p$ $k=40$ keV | $2p$ $k=200$ keV |
|---|---|---|---|---|---|---|---|
| 0 | −0.008 | −0.700 | 0.026 | 0.034 | 0.112 | −0.172 | −0.032 |
| 10 | −0.221 | −0.072 | −0.030 | 0.080 | −0.023 | −0.180 | −0.027 |
| 20 | −0.223 | −0.062 | −0.024 | 0.101 | −0.021 | −0.191 | −0.016 |
| 40 | −0.170 | −0.032 | −0.005 | 0.082 | −0.007 | −0.164 | 0.005 |
| 60 | −0.090 | −0.003 | 0.007 | 0.009 | 0.004 | −0.084 | 0.012 |
| 90 | 0.040 | 0.024 | 0.010 | −0.049 | 0.006 | 0.062 | 0.003 |
| 120 | 0.142 | 0.034 | 0.007 | 0.015 | 0.003 | 0.161 | −0.005 |
| 150 | 0.180 | 0.034 | 0.008 | 0.088 | 0.008 | 0.171 | 0.000 |
| 180 | 0.098 | 0.034 | 0.010 | 0.085 | 0.017 | 0.141 | 0.002 |
| $\sigma_{HFS}$ (b/atom) | 869.2 | 352.1 | 126.7 | 1541 | 39.81 | 1902 | 20.50 |
| $\sigma_{HFS}/\sigma_c$ | 0.9771 | 0.9773 | 0.9791 | 0.8673 | 0.8933 | 0.8261 | 0.8358 |
| $\Xi^2_{HFS}$ | 0.9867 | 0.9867 | 0.9867 | 0.8904 | 0.8904 | 0.8378 | 0.8378 |
| $NE$ | 0.010 | 0.010 | 0.008 | 0.027 | −0.003 | 0.014 | 0.002 |

TABLE V. Expansion coefficients for $Z=6$ Coulomb $1s$.

| $l$ | 1 keV $B(l)$ | 1 keV $B_4(l)$ | 1 keV $BS_4(l)$ | 5 keV $B(l)$ | 5 keV $B_4(l)$ | 5 keV $BS_4(l)$ | 50 keV $B(l)$ | 50 keV $B_4(l)$ | 50 keV $BS_4(l)$ | 100 keV $B(l)$ | 100 keV $B_4(l)$ | 100 keV $BS_4(l)$ |
|---|---|---|---|---|---|---|---|---|---|---|---|---|
| 0 | 1.000 | 1.000 | 1.000 | 1.000 | 1.000 | 1.000 | 1.000 | 1.000 | 1.000 | 1.000 | 1.000 | 1.000 |
| 1 | 0.107 | 0.000 | 0.000 | 0.318 | 0.000 | 0.000 | 1.022 | 0.012 | 0.013 | 1.399 | 0.035 | 0.034 |
| 2 | −0.993 | −1.000 | −1.000 | −0.940 | −1.000 | −1.000 | −0.374 | −0.999 | −1.000 | 0.175 | −1.003 | −1.000 |
| 3 | −0.107 | 0.000 | 0.000 | −0.309 | 0.000 | 0.000 | −0.724 | −0.012 | −0.013 | −0.627 | −0.035 | −0.034 |
| 4 | −0.007 | 0.000 | 0.000 | −0.059 | 0.000 | 0.000 | −0.504 | −0.002 | 0.000 | −0.739 | 0.003 | 0.000 |
| 5 | 0.000 | 0.000 | 0.000 | −0.009 | 0.000 | 0.000 | −0.254 | 0.000 | 0.000 | −0.550 | −0.002 | 0.000 |
| 6 | 0.000 | 0.000 | 0.000 | −0.001 | 0.000 | 0.000 | −0.107 | 0.000 | 0.000 | −0.331 | 0.000 | 0.000 |
| 7 | 0.000 | 0.000 | 0.000 | 0.000 | 0.000 | 0.000 | −0.040 | 0.000 | 0.000 | −0.174 | 0.002 | 0.000 |
| 8 | 0.000 | 0.000 | 0.000 | 0.000 | 0.000 | 0.000 | −0.014 | 0.000 | 0.000 | −0.085 | 0.000 | 0.000 |
| 9 | 0.000 | 0.000 | 0.000 | 0.000 | 0.000 | 0.000 | −0.005 | 0.000 | 0.000 | −0.039 | 0.000 | 0.000 |
| 10 | 0.000 | 0.000 | 0.000 | 0.000 | 0.000 | 0.000 | −0.001 | 0.000 | 0.000 | −0.017 | 0.000 | 0.000 |

TABLE VI. Expansion coefficients for $Z=92$ Coulomb $1s$.

| $l$ | 175 keV $B(l)$ | 175 keV $B_4(l)$ | 175 keV $BS_4(l)$ | 200 keV $B(l)$ | 200 keV $B_4(l)$ | 200 keV $BS_4(l)$ | 400 keV $B(l)$ | 400 keV $B_4(l)$ | 400 keV $BS_4(l)$ |
|---|---|---|---|---|---|---|---|---|---|
| 0 | 1.000 | 1.000 | 1.000 | 1.000 | 1.000 | 1.000 | 1.000 | 1.000 | 1.000 |
| 1 | 0.697 | −0.329 | 0.041 | 0.910 | −0.380 | 0.056 | 1.734 | −0.762 | 0.081 |
| 2 | −0.593 | −0.814 | −1.000 | −0.370 | −0.755 | −1.000 | 1.029 | −0.261 | −1.000 |
| 3 | −0.596 | 0.141 | −0.041 | −0.661 | 0.123 | −0.056 | 0.045 | −0.066 | −0.081 |
| 4 | −0.313 | 0.000 | 0.000 | −0.463 | 0.010 | 0.000 | −0.553 | 0.088 | 0.000 |
| 5 | −0.127 | 0.001 | 0.000 | −0.241 | 0.001 | 0.000 | −0.747 | 0.001 | 0.000 |
| 6 | −0.045 | 0.000 | 0.000 | −0.107 | 0.000 | 0.000 | −0.701 | 0.000 | 0.000 |
| 7 | −0.014 | 0.000 | 0.000 | −0.043 | 0.000 | 0.000 | −0.557 | 0.000 | 0.000 |
| 8 | −0.004 | 0.000 | 0.000 | −0.016 | 0.000 | 0.000 | −0.402 | 0.000 | 0.000 |
| 9 | −0.001 | 0.000 | 0.000 | −0.006 | 0.000 | 0.000 | −0.271 | 0.000 | 0.000 |
| 10 | 0.000 | 0.000 | 0.000 | −0.002 | 0.000 | 0.000 | −0.174 | 0.000 | 0.000 |
| 11 | 0.000 | 0.000 | 0.000 | −0.001 | 0.000 | 0.000 | −0.108 | 0.000 | 0.000 |
| 12 | 0.000 | 0.000 | 0.000 | 0.000 | 0.000 | 0.000 | −0.065 | 0.000 | 0.000 |

$n=4$. For low energies we know that in the screened case $\gamma \neq 1$ and there may be a $\beta$-independent $Z$-dependent piece, but probably the high-energy behavior is more important since that is where the problems in convergence occur. For high energies, however, the dominant term of the Sauter formula corresponds to $n=3$. $Z^2$ corrections fill in the Sauter zero in the forward direction, but a (nonsymmetric) choice of $B_n(l)$ will achieve this. Since screening does not affect the shape of the angular distribution, we may expect screened $B_n$'s to approach point-Coulomb $B_n$'s with increasing energy. Such representations have been used to improve the convergence of partial-wave series for elastic scattering.

We illustrate the improved convergence which can be obtained with convergence factors of the type of Eq. (5.1), for $\gamma=1$ and $n=4$. We give in Tables V and VI for low- and high-$Z$ $K$-shell point-Coulomb cases, the coefficients $B_0(l)$ and $B_4(l)$. For $Z=6$ at 100 keV, we need $B_0(l)$'s from $l=0$ to $l=12$ to obtain results good within about 1% without the transformation of Eq. (5.1), while the reduced series with $\gamma=1, n=4$, requires $B_4(l)$'s only from $l=0$ to $l=4$. A similar result is obtained for the $Z=92$ $K$-shell case at $k=400$ keV. The Sauter results $BS_4(l)$ agree well for the low-$Z$ but not the high-$Z$ case.

## VI. COMPARISON OF THEORY AND EXPERIMENT (REF. 20)

Experimental data on photoelectron angular distributions exists for an energy range which extends up to 2.75 MeV.[21] It is natural for our purpose to divide this range into three regions: high, medium, and low energies. High energies refer to the region from about 100 keV up. Medium energies start at a few keV and extend to about 100 keV, while the low-energy region, for our purpose, starts at a few keV and goes down to about 100 eV or some tens of eV (since we are considering theory within the independent-electron model).[22] In some of the low-energy cases the many-electron effects which we neglect do become important. We give in Table VII our computed binding energies $\epsilon$ for electrons in some subshells of the atoms Ne, Ar, Kr, Xe, and Hg, so that in the low-energy region it will be possible to determine the photoelectron kinetic energy $T_1$ for our calculations at specified photon energies $k$.

There are not many experimental results for photoelectron angular distributions at least 100 eV above threshold. Even fewer can be compared in detail with theoretical computations, owing to the need to apply various corrections to the raw experimental data. These include (a) geometrical corrections of the experimental setup (e.g., finite solid angles subtended by converter at the source) and (b) multiple scattering corrections, since the converter is not an isolated atom but has some thickness. We refer the interested reader to Hultberg[23] and Sujkowski[21] and references therein for the high-energy techniques and to Krause[24] and references therein for the low-energy techniques. Unfortunately many experiments were reported without obtaining these corrections; the "uncorrected" angular distributions cannot be compared quantitatively with our computations. Experimental results which are ratios of quantities having the same correction factors provide an exception, and we have compared our theoretical results with such experimental ratios (cf. Table VIII).

TABLE VII. Computed relativistic Hartree-Fock-Slater binding energies.

| Element | Subshell | Binding energy $\epsilon$ (in eV) |
|---|---|---|
| Neon | $1s$ | 858.15 |
| | $2s$ | 43.23 |
| | $2p_{1/2}$ | 20.08 |
| | $2p_{3/2}$ | 19.96 |
| Argon | $3p_{1/2}$ | 14.62 |
| | $3p_{3/2}$ | 14.43 |
| Krypton | $3s$ | 278.83 |
| | $3p_{1/2}$ | 215.17 |
| | $3p_{3/2}$ | 206.92 |
| | $3d_{3/2}$ | 95.32 |
| | $3d_{5/2}$ | 93.92 |
| | $4s$ | 27.45 |
| | $4p_{1/2}$ | 13.43 |
| | $4p_{3/2}$ | 12.70 |
| Xenon | $5p_{1/2}$ | 12.37 |
| | $5p_{3/2}$ | 10.96 |
| Mercury | $5d_{3/2}$ | 15.98 |
| | $5d_{5/2}$ | 13.92 |
| | $6s$ | 9.57 |

For the sake of completeness we have listed in Table VIII all the experimental data which, to the best of our knowledge, exist for energies greater than 100 eV although we did not compute the uncorrected cases. In Table VIII the experimentally reported values of $\theta_{max}$ (the angle for which the angular distribution attains its maximum) are compared with theory. The table references the figures which make more detailed comparisons between experimental angular distributions and theory.

All the available corrected experimental angular distributions for the high-energy region are shown in Figs. 8 and 9. The data presented concerns $K$-shell angular distributions from high-$Z$ (U, Pb, Bi, and Au), medium-$Z$ (Nd, Ag), and

TABLE VIII. Experimental data on photoelectron angular distributions for photon energies larger than 0.1 keV.

| Author(s) | Ref. | Element | Shell | Parameter measured | $k$ (keV) | Experimental result | Theoretical result |
|---|---|---|---|---|---|---|---|
| Hultberg | 42 | Au | $K$ | $\theta_{max}$ [a] | 412 | 24.0° ± 0.5° [b] | 25.1° |
| | | U | $K$ | $\theta_{max}$ [a] | 662 | 19.5° ± 0.5° [b] | 19.1° |
| | | Pb | $K$ | $\theta_{max}$ [a] | 662 | 19.0° ± 0.5° | 18.2° |
| | | Pb | $K$ | $\theta_{max}$ [a] | 1332 | 11.5° ± 0.5° | 10.1° |
| Hultberg | 23 | U | $K$ | Angular distribution | 412, 662, 1332 | Figs. 8(c) and 9(a) | Figs. 8(c) and 9(a) |
| | | | $L$ | Angular distribution | 412, 662, 1332 | Uncorrected | ··· |
| | | | $M^{+}$ [c] | Angular distribution | 412, 662, 1332 | Uncorrected | ··· |
| Sujkowski | 21 | U | $K$ | Angular distribution | 279 | Fig. 8(c) | Fig. 8(c) |
| | | | $K$ | Angular distribution | 2750 | Uncorrected | ··· |
| | | | $L, M$ | Angular distribution | 103 | Uncorrected | ··· |
| Bergkvist and Hultberg | 26 | Au | $K$ | Angular distribution | 412 | Fig. 8(a) | Fig. 8(a) |
| Bergkvist | 27 | Au | $L$ | Angular distribution | 412 | Fig. 8(a) | Fig. 8(a) |
| Oms and Chedin | 25 | Pb | $K$ | Angular distribution | 279 | Fig. 9(c) | Fig. 9(c) |
| Roy *et al.* | 30 | Al | $K$ | Angular distribution | 1170 | Fig. 9(a) | Fig. 9(a) |
| | | Al | $K$ | Angular distribution | 1332 | Fig. 9(b) | Fig. 9(b) |
| Rimskii-Korsakov *et al.* | 28 | U | $K$ | Angular distribution | 662 | Fig. 9(c) | Fig. 9(c) |
| | | Nd | $K$ | Angular distribution | 662 | Fig. 8(b) | Fig. 8(b) |
| | | Bi | $K$ | Angular distribution | 412 | Fig. 8(b) | Fig. 8(b) |
| | | Bi | $K$ | Angular distribution | 1332 | Fig. 9(b) | Fig. 9(b) |
| Aglintsev *et al.* | 29 | Ag | $K$ | Angular distribution | 662 | Fig. 8(b) | Fig. 8(b) |
| | | Bi | $K$ | Angular distribution | 662 | Fig. 8(b) | Fig. 8(b) |
| Krause | 33 | Kr | $M, N$ | Angular distribution and ratios at 90° | 0.3–1.5 | Fig. 11 and Table X | Fig. 11 and Table X |
| | | Ne | $K$ | Angular distribution and ratios at 90° | 0.3–1.5 | Fig. 12 | Fig. 12 |
| Wuilleumier and Krause | 34 | Ne | $L$ | Angular distribution and ratios at 90° | 0.1–2.0 | Fig. 10 and Tables IX and XI | Fig. 10 and Tables IX and XI |
| Carlsson *et al.* | 35 | Ge | $L$ | $[\sigma_{L_{II}}(90°)+\sigma_{L_{III}}(90°)]/\sigma_{L_I}(90°)$ | 5.4147 | 1.57 ± 0.12 | 1.335 |
| | | | | $[\sigma_{L_{II}}(90°)+\sigma_{L_{III}}(90°)]/\sigma_{L_I}(90°)$ | 8.0478 | 0.99 ± 0.08 | 0.864 |
| Hultberg and Novakov | 43 | Au | $K$ | Angular distribution | 412 | Uncorrected | ··· |
| Hultberg and Sujkowski | 44 | U | $K$ | Angular distribution | 412, 662, 1332 | Uncorrected | ··· |
| | | | $L$ | Angular distribution | 412, 662, 1332 | Uncorrected | ··· |
| | | | $M^{+}$ | Angular distribution | 412, 662, 1332 | Uncorrected | ··· |
| Hultberg *et al.* | 45 | U | $K, I$ | Angular distribution | 1118 | Uncorrected | ··· |
| | | | $M^{+}$ | Angular distribution | | Uncorrected | ··· |
| Frey *et al.* | 46 | U | $K$ | Angular distribution | 208 | Uncorrected | ··· |
| | | | $L$ | Angular distribution | 208, 158 | Uncorrected | ··· |

[a] $\theta_{max}$ is the angle for which the angular distribution is largest.

[b] A careful analysis of the data presented in Refs. 42 and 23 (both in graphs and tables) shows that the value 24.4° for the Au case and 19° for the U case are more consistent with the experimental data presented.

[c] $M^{+}$ indicates values for the $M$ and all higher subshells.

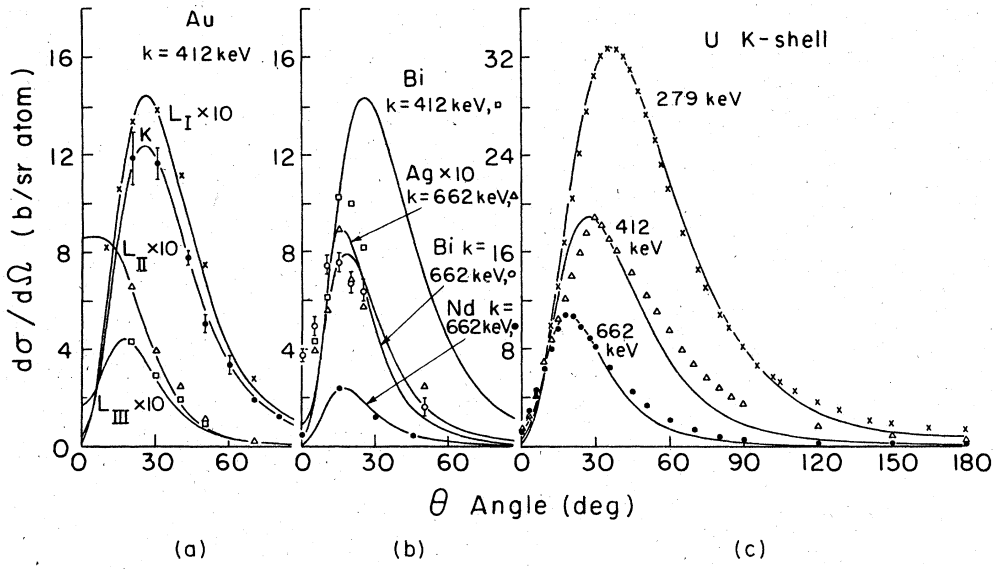


FIG. 8. (a) Angular distributions of gold $K$, $L_I$, $L_{II}$, and $L_{III}$ subshells for $k = 412$ keV. Solid lines are our relativistic HFS computations and circles, crosses, triangles, and squares are the measurements of Bergkvist and Hultberg (Ref. 26, $K$ shell) and of Bergkvist (Ref. 27, $L$ subshells). The error bars, presented for the $K$ shell only, give the claimed experimental error. (b) Angular distributions of neodymium, bismuth and silver $K$ shell photoelectrons for $k = 662$ keV and of bismuth for $k = 412$ keV. Solid lines are our relativistic HFS computations and solid points, circles, triangles, and squares are respectively the measurements of Rimskii-Korsakov and Smirnov (Ref. 28), Aglintsev *et al.* (Ref. 29, Bi and Ag $k = 662$ keV cases) and Rimskii-Korsakov and Smirnov (Ref. 28). The error bars give the claimed experimental error. (c) Angular distributions of uranium $K$-shell photoelectrons for $k = 662$, 412, and 279 keV. Solid lines are our relativistic HFS computations and circles, triangles, and crosses represent the experimental points at the respective energies measured by Hultberg (Ref. 23, first two energies) and by Sujkowski (Ref. 21).

low-$Z$ (Al) targets at 279, 412, 662, 1170, and 1332 keV photon energies and the three $L$ subshells angular distributions from Au at 412 keV. Except for one case (tabular data of Oms and Chedin[25]), which is given in absolute units, all other experimental data are given in arbitrary units. The experimental data (tables of Hultberg,[23] and Sujkowski[21] and graphs of Bergkvist and Hultberg,[26] Bergkvist,[27] Rimskii-Korsakov and Smirnov,[28] Aglintsev *et al.*[29] and Roy *et al.*[30]) are normalized to our computed absolute units at the measured point which is closest to the maximum of the angular distribution. Our computations are represented as lines (solid or broken) and the different experimental points are marked as circles, crosses, etc. (except once in Fig. 9(c), where a broken-dotted line also represents the experimental results). The size of such marks has no implication for the experimental error involved unless an error bar is drawn. The claimed experimental errors are 1%–25%.

The angular distributions in our formulation are given as $(\sigma/4\pi)\sum_n B_n P_n(\cos\theta)$ and the accuracy of the computed total cross section $\sigma$ is better than 0.5%.[31] This is also the accuracy of each of the computed $B_n$'s. Therefore, the largest values of the angular distribution have the same accuracy. However the accuracy of the small values of the angular distribution (relative to its maximum) become worse and can be about 10% when two or three orders of magnitude less than the maximal value. The reason is that these small numbers are linear combinations of large numbers (the $B_n$'s) which are accurate themselves only to about 0.5%.

Inspection of Figs. 8 and 9 shows that in the majority of the cases the agreement between experiment and theory is (either) very good or at least reasonable. This is so for both low and high energies and for small and large atomic numbers. One of the most striking disagreements exists for the experiment of Rimskii-Korsakov and Smirnov [Ref. 28 and solid circles and broken-dotted line in Fig. 9(c)]. However for this particular case we have another measurement by Hultberg[23] in excellent agreement with theory [circles for this experiment and broken line for theory in Fig. 9(c)]. A similar problem arises for the cases shown in Fig. 8(b) (except for neodymium). In Fig. 8(c) we see some discrepancy in the case of

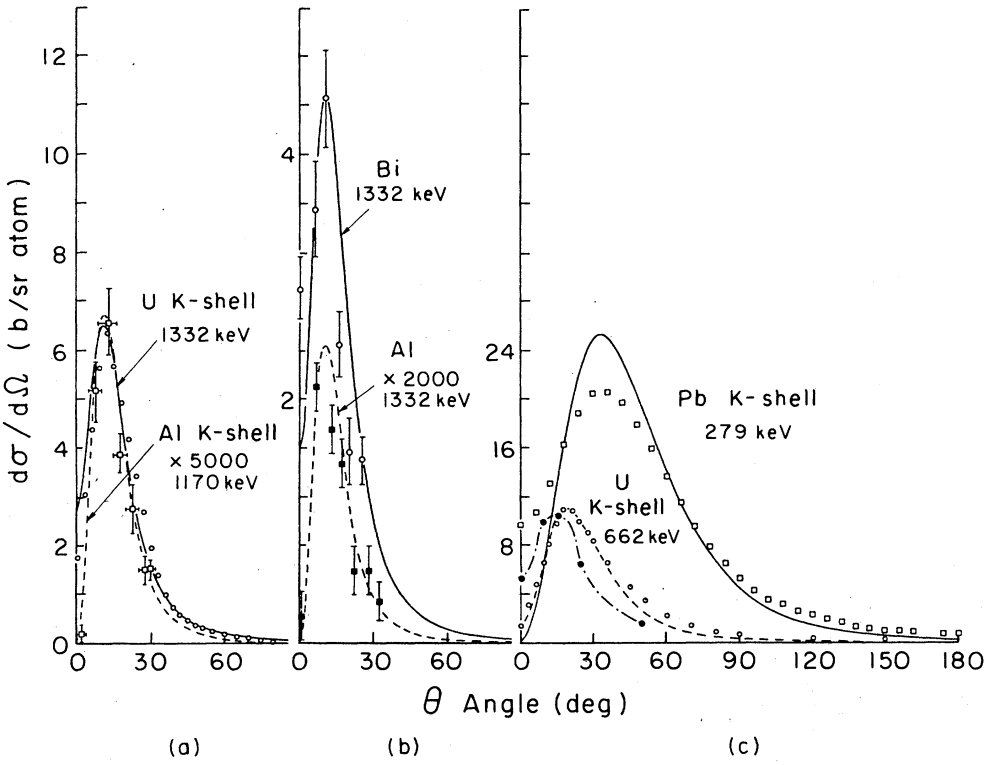


FIG. 9. (a) Angular distributions of $K$-shell photoelectrons of uranium for $k = 1332$ keV (solid line is our relativistic HFS computation and circles are Hultberg's experimental points, Ref. 23) and of aluminum for $k = 1170$ keV (broken line is our relativistic HFS computation and squares, including error bars, are the experimental results of Roy *et al.*, Ref. 30). (b) Angular distributions of $K$-shell photoelectrons of aluminum and bismuth for $k = 1332$ keV. Broken line is our relativistic HFS computation for aluminum and squares are the experimental data of Roy, Goes, and Berger (Ref. 30). Solid line is our computation for bismuth and circles are the experimental points of Rimskii-Korsakov and Smirnov (Ref. 28). Error bars give the claimed experimental accuracy. (c) Angular distributions of lead $K$-shell photoelectrons for $k = 279$ keV and of uranium $K$ shell at $k = 662$ keV. Solid line is our relativistic HFS computation for lead and squares are the experimental points measured by Oms and Chedin (Ref. 25). Broken line is our computation for uranium and circles are Hultberg's (Ref. 23) experimental points. Broken-dotted curve and solid circles are Rimskii-Korsakov and Smirnov's (Ref. 28) experimental data for uranium $K$ shell at $k = 662$ keV.

Hultberg's[23] experiment for the uranium $K$-shell result for $k = 412$ keV. Note, however, that two cases (279 and 662 keV) which agree well bound the 412 keV case. The data of Oms and Chedin[25] for Pb at 279 keV [Fig. 9(c)] shows a shape different from our calculations and from the U data at the same energy. The results of Bergkvist and Hultberg[26] and of Bergkvist[27] for gold $K$, $L_{\mathrm{I}}$, and $L_{\mathrm{II}}$ subshells at the photon energy of 412 keV are shown in Fig. 8(a). The $2s$ shape coincides with the $1s$ shell shape for reasons we have discussed earlier. In fact, the calculated shapes of the $1s$ and $2s$ angular distributions of gold are within 2% for the parts of the angular distributions which are large. Where the distributions have low intensity, the disagreement is 6% at most. For such values (near 0°) the accuracy of the calculation is not much better. All these results show good agreement between experiment and theory.

Summing up the situation for the high-energy region, we can say that in the majority of the cases very good agreement between experiment and theory exists. This agreement is manifest in both ends of this energy interval: the high-energy end (1332 keV) and the low-energy end (279 keV) as well as for heavy ($Z = 92$) and light ($Z = 13$) elements. We believe, in considering individual experiments which disagree with theory and other experiments, that there is no evidence for any systematic disagreement between theory and experiment.

The intermediate range of energy is of interest because we expect to see the breakdown of the normalization screening theory. However the only experiments at these energies were reported by Sobey and Ebert,[32] who measured the $K$-shell

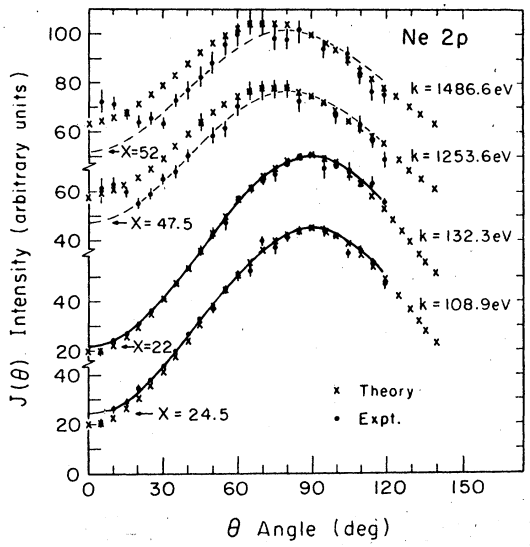


FIG. 10. Comparisons of normalized angular cross sections $J(\theta) \equiv 100\ (d\sigma/d\Omega)(\theta)/(d\sigma/d\Omega)\ (\theta = 90°)$ of Ne $2p$ photoelectrons between the experimental data (solid circles) of Wuilleumier and Krause (Ref. 34) and our relativistic HFS results (crosses). The experimental results were fitted by Wuilleumier and Krause according to $J(\theta) = X + Y \sin^2\theta$ (with $X + Y = 100$) for photon energies $k = 108.9$ and 132.3 eV (solid lines); and according to $J(\theta) = X + Y\ [1 + (5v/c)\cos\theta] \sin^2\theta$ for $k = 1253.6$ and 1486.6 eV (broken lines).

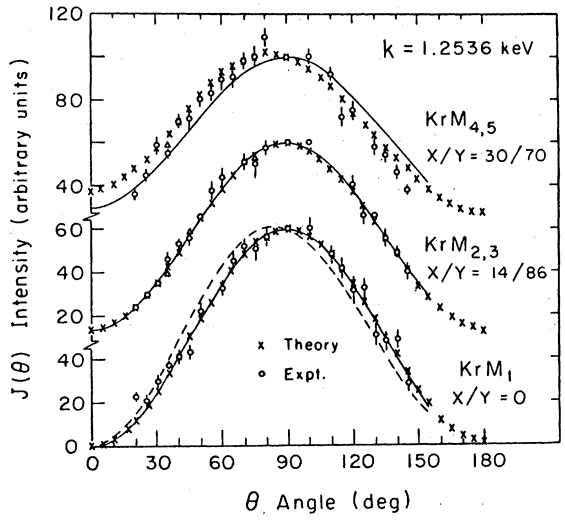


FIG. 11. Comparisons of normalized angular cross section $J(\theta)$ of Kr $3s$, $3p$, and $3d$ photoelectrons for $k = 1.2536$ keV) between the experimental data (circles) of Krause (Ref. 33) and our relativistic HFS results (crosses). The experimental results were fitted by Krause according to $J(\theta) = X + Y \sin^2\theta$ (solid lines) with $X + Y = 100$, and according to $J(\theta) \propto [1 + 4(v/c)\cos\theta] \sin^2\theta$ (broken line).

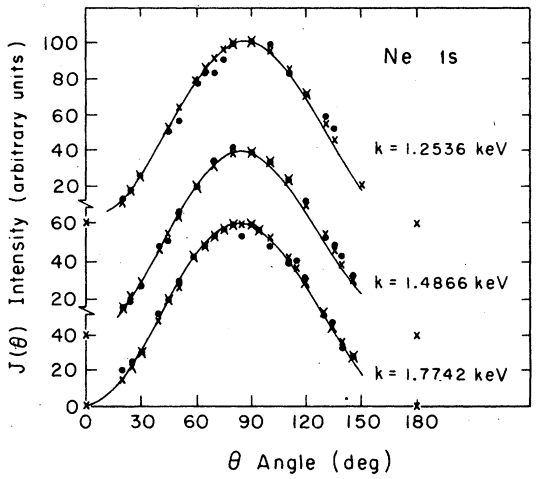


FIG. 12. Comparisons of normalized angular cross sections of Ne $1s$ photoelectrons (for $k = 1.7742$, 1.4866, and 1.2536 keV) between the experimental data (circles) of Krause (Ref. 33) and our relativistic HFS results (crosses). The experimental results were fitted by Karuse to $J(\theta) \propto [1 + 4(v/c)\cos\theta] \sin^2\theta$ (solid lines).

photoelectron angular distributions from both copper and molybdenum using unpolarized monoenergetic x rays in the range of 25–67 keV. Their results cannot be examined in detail owing to residual experimental uncertainties, but generally agree with both computed point-Coulomb and screened predictions (not yet very different) within the accuracy of the experiments.

TABLE IX. Ratios of angular distributions of neon $2s$ and $2p$ subshells at 90° for various photon energies as measured by Wuilleumier and Krause (Ref. 34) and from our computation.

| Photon energy (in eV) | $\sigma_{2s}(90°)/\sigma_{2p}(90°)$ Experiment | Theory |
|---|---|---|
| 108.9 | 0.135 | 0.201 |
| 132.3 | 0.159 | 0.257 |
| 151.4 | 0.177 | 0.301 |
| 171.4 | 0.209 | 0.346 |
| 192.3 | 0.254 | 0.392 |
| 236.9 | 0.36 | 0.491 |
| 260.1 | 0.40 | 0.545 |
| 278.0 | 0.46 | 0.588 |
| 395.3 | 0.70 | 0.880 |
| 452.2 | 0.78 | 1.014 |
| 524.9 | 0.90 | 1.190 |
| 572.8 | 1.04 | 1.309 |
| 929.7 | 1.72 | 2.241 |
| 1253.6 | 2.56 | 3.100 |
| 1486.6 | 3.25 | 3.705 |
| 2042.0 | 4.5 | 5.150 |

TABLE X. Ratios of angular distributions of krypton $3s$, $3p$, $4s$, and $4p$ subshells to the $3d$ subshell at 90° for various photon energies as measured by Krause (Ref. 33) and from our calculation.

| Photon energy (in eV) | $\sigma_{3s}(90°)/\sigma_{3d}(90°)$ Experiment | Theory | $\sigma_{3p}(90°)/\sigma_{3d}(90°)$ Experiment | Theory | $\sigma_{4s}(90°)/\sigma_{3d}(90°)$ Experiment | Theory | $\sigma_{4p}(90°)/\sigma_{3d}(90°)$ Experiment | Theory |
|---|---|---|---|---|---|---|---|---|
| 277 | | | 33 ± 12 | 16 | 2.5 | 1.5 | 4 | 2.5 |
| 452 | 15 ± 6 | 11 | 48 ± 8 | 39 | 3.5 ± 1.2 | 1.75 | 6.0 ± 1.5 | 4 |
| 500 | 21 ± 5 | 9.5 | 44 ± 10 | 35 | | 1.5 | | 4 |
| 525 | 14 ± 2 | 13 | 51 ± 3 | 48 | 2.8 ± 0.4 | 2 | 5.2 ± 0.5 | 5 |
| 573 | | 11.5 | 49 ± 8 | 43 | 3.5 | 1.75 | 5.5 | 4.5 |
| 705 | 17 ± 7 | 18.5 | 75 ± 10 | 70.5 | 7 | 2.7 | 15 | 6.5 |
| 852 | 15 ± 5 | 24 | 89 ± 8 | 90 | 6 | 3.3 | 10 | 8 |
| 930 | 20.8 ± 1.5 | 27.2 | 95.5 ± 2.5 | 100 | 3.8 ± 0.6 | 3.75 | 9.7 ± 0.8 | 9 |
| 1012 | 20 ± 3 | 30.5 | 106 ± 6 | 111 | 7 | 4 | 9 | 10 |
| 1254 | 35 ± 3 | 42 | 128 ± 6 | 143 | | 5.5 | | 12.5 |
| 1487 | 50 ± 15 | 55 | 160 ± 15 | 175 | | 7 | | 15 |

At lower energies, but staying generally some 100 eV above threshold, it is possible to compare with the extensive experiments of Krause[33] for the $3s$, $3p$, $3d$, $4s$, and $4p$ subshells of krypton at various photon energies in the range of 277–1487 eV and for the $K$ shell of neon at the energies 1253.6, 1486.6, and 1774.2 eV; the extensive experiments of Wuilleumier and Krause[34] for the $2s$ and $2p$ subshells of neon in the photon energy range of 108.9–2042 eV, and the experiment of Carlsson *et al.*,[35] who give ratios of the $2p$ subshells of Ge to $2s$ at 90° at the photon energies $k = 5.4147$ and $k = 8.0478$ keV. The results for the latter case are shown in Table VIII. The experimental results differ from our theoretical values by about 14%–17%, whereas the claimed experimental error is about 8%. Figures 10–12 show the experimental and theoretical shapes of the angular distributions for ten cases for which very detailed experimental data of Krause[33] and of Wuilleumier and Krause[34] exist. The rest of their measurements are less detailed and will be discussed separately. A striking feature is the deviation of the experimental angular distributions from the NR dipole formula 2.11 (which can also be written as $d\sigma/d\Omega = X + Y\sin^2\theta$), even for energies as low as 1.254 keV. Our computations agree with experimental results at least as well as NR dipole and usually better. In Fig. 10 one sees very good agreement between experiment and our calculation for $k = 1486.6$ and $k = 1253.6$ eV at angles starting at 180° and down to about 55°. These experiments confirm our expectation from Sec. III that NR dipole formulas should be used with caution even when dealing with low-energy light-atom cases.

Tables IX and X compare theory with further results of these experiments for the ratios of the various angular distributions at 90° at many energies. The rations $\sigma_{2s}(90°)/\sigma_{2p}(90°)$ for neon (Ref. 34) are compared in Table IX and the ratios

TABLE XI. Angular distribution ratio $\sigma_{2s}(\theta_0)/\sigma_{2p}(\theta_0)$ at $\theta_0 = 54°44'$ and asymmetry parameter, $\beta_{21}$ for the $2p$ subshell. Experimental data of Wuilleumier and Krause (Ref. 34) and theoretical results of Kennedy and Manson (Ref. 36, referred as KM) and our calculations ("Present theory").

| Photon energy (in eV) | $\sigma_{2s}(\theta_0)/\sigma_{2p}(\theta_0)$ Experiment | Present theory | $\beta_{21}$ Experiment[a] | KM | Present theory |
|---|---|---|---|---|---|
| 108.9 | 0.118 | 0.181 | 1.35 | 1.40 | 1.46 |
| 132.3 | 0.145 | 0.229 | 1.41 | 1.45 | 1.49 |
| 151.4 | 0.169 | 0.267 | 1.49 | 1.45 | 1.49 |
| 236.9 | 0.320 | 0.425 | [1.42] | 1.42 | 1.44 |
| 278.0 | 0.360 | 0.503 | [1.40] | 1.41 | 1.41 |
| 929.7 | 1.46 | 1.75 | [0.98] | 0.87 | 0.89 |
| 1253.6 | 2.1 | 2.36 | 0.85 | 0.74 | 0.74 |
| 1486.6 | 2.6 | 2.79 | 0.76 | 0.64 | 0.66 |

[a] Values in square brackets are interpolated and based upon the trend of the Kennedy-Manson calculation.

TABLE XII. Comparison between exact numerical total cross section and results of Eq. (6.1) for neon and krypton. Here $a(n)$ means $a \times 10^n$.

| | | | Photoeffect cross section in barns/atom | | |
|---|---|---|---|---|---|
| | | $k$ | | Approx. | Approx. |
| $Z$ | Subshell | (keV) | This work | Eq. (6.1) | This work |
| 10 | $2p$ | 0.1089 | 2.86(6) | 2.91(6) | 1.02 |
| | | 0.1323 | 1.86(6) | 1.91(6) | 1.03 |
| | | 1.2536 | 2.52(3) | 2.87(3) | 1.14 |
| | | 1.4866 | 1.40(3) | 1.62(3) | 1.16 |
| 36 | $3s$ | 1.2536 | 2.99(4) | 2.99(4) | 1.00 |
| | $3p$ | 1.2536 | 1.08(5) | 1.09(5) | 1.01 |
| | $3d$ | 1.2536 | 8.21(4) | 9.20(4) | 1.12 |

at 90° of the $3s$, $3p$, $4s$, and $4p$ subshells of krypton relative to the $3d$ subshell (Ref. 33) are compared in Table X. Reasonably good agreement between theory and experiment is shown for krypton; for neon there is considerable disagreement in the lower-energy range. When Wuilleumier and Krause[34] compared their Ne data with theoretical calculations of Kennedy and Manson,[36] who made a NR computation but used HF wave functions, they found agreement at the lower energies, becoming worse as energy increases. This suggests that at low-energies many-electron effects, which are dealt with more appropriately using HF wave functions, are important and our omission of these effects leads to disagreement. However when energies increase, since these effect tend to disappear and corrections to NR dipole approximation become important, we get better agreement with experiment than Kennedy and Manson.[36] This is confirmed in the comparisons Wuillemier and Krause[34] make with work which takes into account many electron effects (Amusia *et al.*,[37] Kelly,[38] and Chang *et al.*[39]). Very good agreement at low energies is then achieved. Table XI shows the neon results (Ref. 34) for the ratio $\sigma_{2s}(\theta)/\sigma_{2p}(\theta)$ at the "magic" angle 54°44′ (see following paragraph) and the asymmetry parameter, $\beta_{21}$ for the $2p$ subshell. The experimental values of the asymmetry parameter agree very well with both Kennedy and Manson[36] and our computations. The ratios at the "magic" angle do not agree so well, but they show the same trend as the experimental results. In fact, the results agree quite nicely for the higher energies and agreement gets worse as the energy drops to its lowest value of 108.9 eV.

Samson and Gardner[40] suggested using the fact that $P_2(\cos 54° 44') = 0$ to transform Eq. (2.11) to

$$(d\sigma/d\Omega)_{54°44'} = \sigma/4\pi. \tag{6.1}$$

TABLE XIII. The asymmetry parameter $\beta_{nL}$ as measured by Niehaus and Ruf (Ref. 30) and from our calculation.

| Element | Subshell | Kinetic energy of photoelectron (eV) | $\beta_{nL}$ Experiment | Theory |
|---|---|---|---|---|
| Ar | $3p_{3/2}$ | 5.457 | 0.95 ± 0.02 | 1.408 |
| | $3p_{1/2}$ | 5.280 | 0.95 ± 0.02 | 1.387 |
| | $3p_{3/2}$ | 1.089 | 0.31 ± 0.03 | 0.584 |
| | $3p_{1/2}$ | 0.734 | 0.25 ± 0.05 | 0.501 |
| Kr | $4p_{3/2}$ | 7.218 | 1.37 ± 0.02 | 1.592 |
| | $4p_{1/2}$ | 6.552 | 1.37 ± 0.03 | 1.532 |
| | $4p_{3/2}$ | 2.849 | 0.91 ± 0.03 | 1.088 |
| | $4p_{3/2}$ | 2.672 | 0.83 ± 0.04 | 1.054 |
| | $4p_{1/2}$ | 2.183 | 0.79 ± 0.03 | 0.964 |
| | $4p_{1/2}$ | 2.006 | 0.72 ± 0.04 | 0.927 |
| Xe | $5p_{3/2}$ | 9.090 | 1.71 ± 0.02 | 1.893 |
| | $5p_{1/2}$ | 7.784 | 1.64 ± 0.06 | 1.803 |
| | $5p_{3/2}$ | 4.721 | 1.45 ± 0.03 | 1.658 |
| | $5p_{3/2}$ | 4.544 | 1.37 ± 0.06 | 1.642 |
| | $5p_{1/2}$ | 3.415 | 1.29 ± 0.04 | 1.511 |
| | $5p_{1/2}$ | 3.238 | 1.20 ± 0.08 | 1.489 |
| Hg | $6s$ | 10.780 | 1.68 ± 0.1 | 0.842 |
| | $6s$ | 1.393 | 2.13 ± 0.1 | 1.641 |
| | $6s$ | 1.193 | 1.25 ± 0.1 | 1.653 |
| | $5d_{5/2}$ | 6.377 | 0.03 ± 0.1 | −0.248 |
| | $5d_{5/2}$ | 2.008 | 0.68 ± 0.1 | 0.421 |
| | $5d_{3/2}$ | 4.513 | 0.25 ± 0.1 | 0.192 |

Thus one would obtain the total cross section by measuring the photoelectron intensity at this particular "magic" angle. However, as Krause[24] already remarked, if the angular distribution deviated from NR dipole approximation Eq. (6.1) is incorrect. We illustrate this in Table XII. Evidently before using Eq. (6.1) one must verify that NR dipole approximation is satisfied.

As a last example we present a case which shows clearly the breakdown of both the relativistic HFS potential model and the dipole approximation. The results of the experiments of Nichaus and Ruf[15] together with our computations are shown in Table XIII. We do not expect our relativistic HFS potential to yield valid results at such low energies, but although the quantitative agreement is not too good we do get some qualitative results and the trends follow the experiment. This is seen clearly for the Kr and Xe results. For the 6*s* case of mercury one sees that even for such low energy (10.78 eV) the dipole approximation value $\beta_{60}=2$ is not obtained both experimentally and in our computation. The value which we calculate,[41] 0.842, is closer to that Niehaus and Ruf[15] find for the pure *jj* coupling: 0.696. For the mercury $5d_{5/2}$ case with $T=6.377$ eV we even get a negative value for $\beta_{52}$. Note that the experimental result of $0.03\pm0.1$ does not exclude a negative value. The HF computations of Kennedy and Manson,[36] which describe better the electronic potential but are of the NR dipole type, agree with these experiments better than our results but still fail to give good agreement.

In conclusion we may say that the experimental evidence does confirm the discussions of angular distributions which we have presented here and previously.[31] At high energies, in accord with the normalization screening theory, angular-distribution shapes are not affected by screening and 1*s* and 2*s* shapes are the same. In the low-energy region NR dipole approximation is not always appropriate, even in the case of low energies and light atoms. This results from relativistic and multipole effects which are also important in the case of heavy elements even close to thresholds.

## ACKNOWLEDGMENTS

This research was supported in part by the National Science Foundation under Grant Nos. PHY74-83531 A03 and 01P7503599, and in part by the National Science Council, Republic of China.

---

*Present address: M division, Lawrence Livermore Laboratory, Box 808, Livermore, Calif. 94550.

[1]R. H. Pratt, A. Ron, and H. K. Tseng, Rev. Mod. Phys. 45, 273 (1973); R. D. Schmickley and R. H. Pratt, Phys. Rev. 164, 104 (1967); point-Coulomb *K*-shell results had also been obtained by S. Hultberg, B. Nagel, and P. O. M. Olsson, Ark. Fys. 38, 1 (1968).

[2]J. W. Cooper and S. T. Manson, Phys. Rev. 177, 157 (1969); D. J. Kennedy and S. T. Manson, Phys. Rev. A 5, 227 (1972); A. F. Starace, S. T. Manson, and D. J. Kennedy, Phys. Rev. A 9, 2453 (1974); D. Dill, A. F. Starace, and S. T. Manson, Phys. Rev. A 11, 1596 (1975).

[3]J. W. Cooper and S. T. Manson, Phys. Rev. 177, 157 (1969); H. A. Bethe, *Handbuch der Physik*, edited by H. Geiger and K. Sheel (Springer-Verlag, Berlin, 1933), Vol. 24/1, p. 482; J. Cooper and R. N. Zare, *Lectures in Theoretical Physics*, edited by S. Geltman, K. Mahantrappa, and W. Brittin (Gordon and Breach, New York, 1969), Vol. IIC, p. 317; S. T. Manson, J. Electron Spectrosc. 1, 413 (1973).

[4]G. Schur, Ann. Phys. (Leipz.) 4, 433 (1930).

[5]H. A. Bethe and E. E. Salpeter, *Quantum Mechanics of One and Two-Electron Atoms* (Academic, New York, 1957).

[6]D. Dill, S. T. Manson, and A. F. Starace, Phys. Rev. Lett. 32, 971 (1974); D. Dill, A. F. Starace, and S. T. Manson, Phys. Rev. A 11, 1596 (1975).

[7]R. H. Pratt, A. Ron, and H. K. Tseng, Rev. Mod. Phys. 45, 273 (1973); R. H. Pratt and H. K. Tseng, Phys. Rev. A 5, 1063 (1972).

[8]F. Sauter, Ann. Phys. (Leipz.) 9, 217 (1931); 11, 454 (1931).

[9]R. H. Boyer, Ph.D. thesis (Oxford University, 1957), (unpublished); T. A. Weber and C. J. Mullin, Phys. Rev. 126, 615 (1962); B. Nagel, Ark. Fys. 24, 151 (1963).

[10]A. F. Starace, R. H. Rast, and S. T. Manson, Phys. Rev. Lett. 38, 1522 (1977).

[11]T. E. H. Walker and J. T. Waber, Phys. Rev. Lett. 30, 307 (1973); J.Phys. B 6, 1165 (1973); 7, 674 (1974).

[12]W. Heitler, *Quantum Theory of Radiation* (Oxford U. P., Oxford, 1954).

[13]J. Fischer, Ann. Phys. (Leipz.) 8, 821 (1931); 11, 489 (1931).

[14]These corrections are not of the form Cooper and Manson had suggested indicating that Cooper and Manson's assumptions for this correction were not appropriate.

[15]A. Niehaus and M. W. Ruf, Z. Phys. 252, 84 (1972).

[16]James McEnnan, L. D. Kissel, and R. H. Pratt, Phys. Rev. A 13, 532 (1976).

[17]Sung Dahm Oh, James McEnnan, and R. H. Pratt, Phys. Rev. A 14, 1428 (1976).

[18]J. McEnnan, D. J. Botto, R. H. Pratt, D. Bunaciu, and V. Florescu, Phys. Rev. A 16, 1768 (1977).

[19]Adam Bechler and R. H. Pratt (to be published).

[20]A preliminary comparison of theory and experiment has recently been reported [A. Ron, R. H. Pratt, and H. K. Tseng, Chem. Phys. Lett. 47, 377 (1977)]. The present section, therefore, attempts a comprehensive survey for energies above 100 eV.

[21]Z. Sujkowski, Ark. Fys. 20, 269 (1961).

[22]D. Liberman, D. T. Cromer, and J. T. Waber, Comput. Phys. Commun. 2, 107 (1971); D. Liberman, J. T. Waber, and D. T. Cromer, Phys. Rev. 27, A137 (1965).

[23]S. Hultberg, Ark. Fys. 15, 307 (1959).
[24]M. O. Krause, *Electron Spectrometry*, *Atomic Inner-Shell Processes*, *Vol. II*, *Experimental Approaches and Applications*, edited by Bernd Crasemann (Academic, New York, 1975), p. 33.
[25]J. Oms and P. Chedin, J. Phys. (Paris) 28, 281 (1967).
[26]K. E. Bergkvist and S. Hultberg, Ark. Fys. 27, 321 (1964).
[27]K. E. Bergkvist, Ark. Fys. 27, 483 (1964).
[28]A. A. Rimskii-Korsakov and V. V. Smirnov, Sov. Phys.-JETP 15, 47 (1962); Bull. Acad. Sci. USSR Phys. Ser. 26, 1180 (1962).
[29]K. K. Aglintsev, V. V. Mitrofanov, A. A. Rimskii-Korsakov, and V. V. Smirnov, Bull. Acad. Sci. USSR Phys. Ser. 25, 1146 (1961).
[30]R. R. Roy, M. L. Goes, and J. Berger, C. R. Acad. Sci. 241, 1936 (1955).
[31]R. H. Pratt, A. Ron, and H. K. Tseng, Rev. Mod. Phys. 45, 273 (1973).
[32]T. M. Sobey and P. J. Ebert, Bull. Am. Soc. 15, 1338 (1970).
[33]M. O. Krause, Phys. Rev. 177, 151 (1969).
[34]F. Wuilleumier and M. O. Krause, Phys. Rev. A 10, 242 (1974).
[35]R. Carlsson, A. Fahlman, and K. Siegbahn, Ark. Fys. 32, 103 (1966).
[36]D. S. Kennedy and S. T. Manson, Phys. Rev. A 5, 227 (1972).
[37]M. Ya Amusia, V. K. Ivanov, N. A. Cherepkov, and L. V. Chernysheva, Phys. Lett. A 40, 361 (1972).
[38]H. P. Kelly, Phys. Rev. A 6, 1048 (1972).
[39]T. N. Chang, T. Ishihara, and R. T. Poe, Phys. Rev. Lett. 27, 838 (1971).
[40]J. A. R. Samson and J. L. Gardner, J. Opt. Soc. Am. 62, 856 (1972).
[41]The value which we had given in Ref. 20 is incorrect.
[42]S. Hultberg, Ark. Fys. 9, 245 (1955).
[43]S. Hultberg and T. Novakov, Nucl. Phys. 4, 120 (1957).
[44]S. Hultberg and Z. Sujkowski, Phys. Rev. Lett. 3, 227 (1959).
[45]S. Hultberg, T. O'Connor, and J. H. Hamilton, Nucl. Phys. 22, 306 (1961).
[46]W. F. Frey, J. H. Hamilton, and S. Hultberg, Ark. Fys. 24, 503 (1963).